Hydrological cycle changes explain weak Snowball Earth storm track despite increased surface baroclinicity

T. A. Shaw[1] and R. J. Graham[2]

[1]Department of the Geophysical Sciences, The University of Chicago, 5734 South Ellis Ave., Chicago, IL, 60637
[2]Department of Physics, The University of Oxford, Oxford, UK

Key Points:

- Snowball Earth storm track is weaker than modern consistent with hydrological cycle changes despite increased surface baroclinicity.
- Weak storm track explained by decreased latent heat flux and meridional surface moist static energy gradient following Clausius-Clapyeron.
- Weak storm track also explained by decreased latent heat release aloft in the tropics (decreased Mean Available Potential Energy).

Corresponding author: Tiffany A. Shaw, tas1@uchicago.edu

Abstract

Simulations show storm tracks were weaker during past cold, icy climates relative to the modern climate despite increased surface baroclinicity. Previous work explained the weak storm track using dry zonally-asymmetric mechanisms associated with orographic forcing. Here we show zonally-symmetric changes in the hydrological cycle explain the weak Snowball Earth storm track. According to the moist static energy framework, the weak storm track is connected to decreased latent heat flux (evaporation) and meridional surface moist static energy gradient. The weak storm track can be predicted using the Clausius-Clapeyron relation and a surface ice albedo. The weak storm track is also consistent with decreased latent heat release aloft in the tropics, which decreases upper-tropospheric baroclinicity and Mean Available Potential Energy, and is significantly correlated with the meridional surface moist static energy gradient. Our insights may apply to other climates such as the Last Glacial Maximum.

Plain Language Summary

Storm tracks (low and high pressure weather systems) dominate Earth's climate in the middle latitudes. Several modern theories connect storm track intensity to the equator-to-pole near-surface temperature gradient. However, it has been known for some time that this connection fails when applied to simulations of past cold, icy climates such as the Last Glacial Maximum and Snowball Earth. Previous work has explained the weak storm track using dry longitudinally-dependent dynamical mechanisms associated with orographic forcing. Here we show the weak Snowball Earth storm track can be explained by hydrological cycle changes that are independent of longitude. In particular, the weak storm track is consistent with decreased evaporation (latent heat flux) and decreased surface equator-to-pole moist static energy gradient, which follow the Clausius-Clapyeron relation. The decreased surface moist static energy gradient is correlated with decreased latent heat release aloft in the tropics, which weakens the potential energy that is available to be converted into kinetic energy.

1 Introduction

Storm tracks are regions where midlatitude cyclones occur most frequently and several modern theories connect their intensity to (near-) surface baroclinicity (meridional temperature gradient) (Chang et al., 2002; Shaw et al., 2016; Held, 2018). The surface baroclinicity-intensity connection is supported by the seasonality of storm track intensity in modern reanalysis data (see Fig. S5 in O'Gorman, 2010) and idealized simulations of annual-mean storm track intensity across a range of climates without ice (see Fig. 4 in O'Gorman & Schneider, 2008) (see Fig. 1 in Caballero & Langen, 2015). It is also assumed in Energy Balance Models (EBMs) (North, 1975; Mbengue & Schneider, 2018). However, it has been known for some time that the surface baroclinicity-intensity connection fails when applied to simulations of past cold, icy climates such as the Last Glacial Maximum (LGM) and Snowball Earth (Hall et al., 1996; Pierrehumbert, 2005; Li & Battisti, 2008). The Snowball Earth hypothesis proposes that during Neoproterozoic glaciations ($\sim$710 and $\sim$ 635 Ma) ice covered most of the planet, possibly to the equator (Hoffman et al., 2017).

Several mechanisms have been proposed to explain why the Northern Hemisphere (NH) wintertime Atlantic storm track during the LGM is weaker than modern despite increased surface baroclinicity. All of the mechanisms are based on dry zonally-asymmetric dynamics, e.g. they appeal to changes in stationary wave amplitude (Hall et al., 1996), reflection (Lofverstrom et al., 2016) and structure (Riviere et al., 2018) due to the orographic forcing of the continental ice sheets or changes in upstream seeding (Donohoe & Battisti, 2009). The NH wintertime zonal-mean Snowball Earth storm track is weaker than modern (Pierrehumbert, 2005). While stationary eddies are also weaker (reduced

land-sea contrast, see Graham et al., 2019), the storm track weakening is so large (∼4 PW, see Fig. 7 in Pierrehumbert, 2005) alternative mechanisms are needed.

The most radical difference between the Snowball Earth and modern climates is the hydrological cycle (Pierrehumbert, 2002). Snowball Earth is cold and dry (evaporation and surface latent heat flux are small over ice) and the surface (ice) albedo is large. Previous work showed the transition from warm and wet to cold and dry climates in zonally-symmetric aquaplanet simulations leads to decreased storm track intensity via increased midlatitude dry static stability (decreased latent heat release aloft) that decreases Mean Available Potential Energy (MAPE, O'Gorman & Schneider, 2008; Schneider et al., 2010). However, those simulations did not include ice, which is fundamental to the Snowball Earth climate. The transition from ocean and land to ice everywhere leads to a reduction of surface latent heat flux and an increase of surface albedo, which both affect the Moist Static Energy (MSE) budget of the atmosphere. Shaw et al. (2018) recently developed a MSE framework for zonal-mean storm track intensity, which includes external parameters that can form the basis of predictions and scaling estimates. For example, Shaw et al. (2018) predicted seasonal storm track intensity using top-of-atmosphere (TOA) insolation and Barpanda and Shaw (2020) used a scaling analysis to derive a critical mixed layer depth that separates large and small storm track seasonality.

Here we examine whether zonally-symmetric mechanisms associated with the hydrological cycle can explain why the Snowball Earth storm track is weaker than modern despite increased surface baroclinicity. We simulate a hard Snowball Earth (ice everywhere) and quantify the impact of the hydrological cycle via changes in surface boundary conditions (decreased latent heat flux and increased surface albedo) using the MSE framework and changes in thermal structure aloft (increased dry static stability) using the MAPE framework. Furthermore, we use the MSE framework to predict a weaker storm track assuming the hydrological cycle changes follow the Clausius-Clapeyron relation and there is a surface (ice) albedo everywhere.

2 Methods

2.1 MSE framework

The MSE framework for storm track intensity can be derived from the zonal-mean atmospheric MSE budget with the global mean removed:

$$\nabla \cdot F_{TE} = \nabla \cdot F_{NE} - \nabla \cdot F_{SC} \tag{1}$$

(see (2) in Kang et al., 2008), where $F_{TE} = \langle[\overline{v'm'}]\rangle$ and $F_{SC} = \langle[\overline{v}\ \overline{m}]\rangle$ are the MSE flux by transient eddies and stationary circulation (mean meridional circulation plus stationary eddies), respectively, F_{NE} is the flux form (global mean removed) of net energy input NE, i.e. $\nabla \cdot F_{NE} = NE$, $\langle\cdot\rangle$ denotes a mass-weighted vertical integration, $[\cdot]$ denotes a zonal average and $\bar{\cdot}$ denotes a monthly average, i.e. an average over a particular month not the climatological monthly average. Similar results are obtained using a 10-day high pass filter (Shaw et al., 2018). The global mean is removed to emphasize meridional gradients (see Kang et al., 2008; Donohoe & Battisti, 2012; Shaw et al., 2018; Donohoe et al., 2020).

An equation for storm track intensity I (unit PW) is derived by multiplying (1) by $2\pi a^2 \cos\phi$ where a is the radius of the Earth and ϕ is latitude and integrating between the pole and the storm track position ϕ_s (where $\nabla \cdot F_{TE} = 0$):

$$I = 2\pi a \cos\phi_s F_{TE}|_{\phi_s} = I_{NE} - I_{SC} \tag{2}$$

$$= 2\pi a \cos\phi_s \left[F_{NE}|_{\phi_s} - F_{SC}|_{\phi_s}\right] \tag{3}$$

(Shaw et al., 2018). Consequently, a storm track intensity change (δI) is connected to changes in net energy input (δI_{NE}) or MSE flux by the stationary circulation (δI_{SC}):

$$\delta I = \delta I_{NE} - \delta I_{SC}. \tag{4}$$

In order to quantify and predict the impact of hydrological cycle changes on storm track intensity we decompose net energy input as follows

$$\begin{aligned} \delta I_{NE} &= \delta I_{THF} + \delta I_{SWABS} - \delta I_{GHE} - \delta I_{\partial h/\partial t} & (5)\\ &= 2\pi a \cos\phi_s \left[\delta F_{THF}|_{\phi_s} + \delta F_{SWABS}|_{\phi_s} - \delta F_{GHE}|_{\phi_s} - \delta F_{\partial h/\partial t}|_{\phi_s}\right] & (6) \end{aligned}$$

where THF is the turbulent heat flux (sensible SH plus latent LH heat flux), SWABS is the shortwave absorption (TOA minus surface shortwave radiation), GHE is the greenhouse effect (surface minus TOA longwave radiation), $\partial h/\partial t$ is atmospheric storage where $h = c_p T + L_v q$ is specific enthalpy and all terms are in flux form (global mean removed), e.g. $\nabla \cdot \delta F_{THF} = \delta THF$.

We can predict the impact of hydrological cycle changes on storm track intensity between the Snowball Earth and modern climates using the MSE framework and the Clausius-Clapeyron relation. The fractional humidity change between different climates following the Clausius-Clapeyron relation is:

$$\frac{\delta q_s^*}{q_{s,M}^*} \approx \frac{\delta e_s}{e_{s,M}} = \exp\left[\frac{L_v}{R_v}\left(\frac{\delta T}{T_S T_M}\right)\right] - 1 = \gamma \tag{7}$$

where q_s^* is the saturation specific humidity, e_s is the saturation water vapor pressure and the subscripts M and S refer to the modern and Snowball Earth climates, respectively (Held & Soden, 2006; Schneider et al., 2010; Boos, 2012). Using representative global-mean temperatures for the Snowball Earth ($T_S \approx 245$ K) and modern ($T_M \approx 285$ K) climates the humidity decrease implied from (7) is approximately 95% ($\gamma \approx -0.95$).

Here we predict the impact of the hydrological cycle via surface boundary condition changes on Snowball Earth storm track intensity. While we expect hydrological cycle changes will also impact the greenhouse effect (via a colder global-mean temperature), it is not clear how the meridional structure of temperature will change because it is affected by the storm track itself. Thus, we cannot easily predict δI_{GHE}. Along similar lines it is not easy to predict δI_{SC} and $\delta I_{\partial h/\partial t}$. Hence we assume δI_{GHE}, δI_{SC} and $\delta I_{\partial h/\partial t}$ are small and focus on predicting δI_{THF} and δI_{SWABS}.

Assuming the change in turbulent heat flux between the Snowball Earth and modern climates is dominated by latent heat flux and the latent heat flux follows changes in saturation specific humidity then

$$\begin{aligned} \delta THF &= \delta(LH + SH) \approx \delta LH & (8)\\ \frac{\delta LH_p}{LH_M} &\approx \frac{\delta q_s^*}{q_{s,M}^*} - \frac{\delta H}{(1 - H_M)} \approx \frac{\delta q_s^*}{q_{s,M}^*} = \gamma & (9) \end{aligned}$$

where the p subscript refers to prediction and H is relative humidity (Schneider et al., 2010). The predicted intensity change is

$$\delta I_{THF,p} = 2\pi a \cos\phi_s \delta F_{LH,p}|_{\phi_s} \tag{10}$$

where $\nabla \cdot \delta F_{LH,p} = \delta LH_p$ is the flux form (global-mean removed). Since $\gamma < 0$ the equator-to-pole gradient of δLH_p is positive (Supplementary Fig. 1a,b) implying $\delta I_{THF,p} < 0$, i.e. a weakening of the storm track.

Shortwave absorption depends on downward TOA ($S_T^{\downarrow}$) and surface ($S_S^{\downarrow}$) shortwave radiation and the surface (α_s) and planetary (α_p) albedos, i.e. $SWABS = (1-\alpha_p)S_T^{\downarrow} -$

$(1-\alpha_s)S_S^{\downarrow}$. Assuming Snowball Earth shortwave absorption depends on surface ice albedo, shortwave optical depth $[\tau_S = -\ln(S_{S,S}^{\downarrow}/S_{T,S}^{\downarrow})]$, and unchanged TOA shortwave radiation, i.e. $SWABS_S = (1 - e^{-2\tau_S}\alpha_{s,S})S_{T,M}^{\downarrow} - (1-\alpha_{s,S})e^{-\tau_S}S_{T,M}^{\downarrow}$, then

$$\delta SWABS_p = -(\alpha_{s,S}e^{-2\tau_S} - \alpha_{p,M})S_{T,M}^{\downarrow} - (1-\alpha_{s,S})e^{-\tau_S}S_{T,M}^{\downarrow} + (1-\alpha_{s,M})S_{S,M}^{\downarrow} \quad (11)$$

The predicted intensity change is

$$\delta I_{SWABS,p} = 2\pi a \cos\phi_s \delta F_{SWABS,p}|_{\phi_s} \quad (12)$$

where $\nabla \cdot \delta F_{SWABS,p} = \delta SWABS_p$ is the flux form (global-mean removed). If we assume the Snowball Earth shortwave optical depth decreases following the Clausius-Clapeyron relation, i.e. $\tau_S \approx (1+\gamma)\tau_M = 0.05\tau_M$, and the surface ice albedo is $\alpha_{s,S} = 0.6$ in AGCM and $\alpha_{s,S} = 0.8$ in AQUA then the equator-to-pole gradient of $\delta SWABS_p$ is positive (Supplementary Fig. 1c,d) implying $\delta I_{SWABS,p} < 0$, i.e. a weakening of the storm track. Note for both predictions (10) and (12) the storm track position is assumed to be fixed to its modern value following previous work (Shaw et al., 2018). We use the simulations discussed in section 2.3 to test the assumptions and predictions by diagnosing all the terms in the MSE framework.

2.2 MAPE framework

Storm track intensity defined using eddy kinetic energy is linearly related to MAPE in idealized simulations and reanalysis data (O'Gorman & Schneider, 2008; O'Gorman, 2010; Gertler & O'Gorman, 2019). Here we calculate MAPE following equation (3) in O'Gorman and Schneider (2008):

$$MAPE = \frac{\kappa c_p}{2g}\frac{1}{p_0^{\kappa}}\int_{p_t}^{850\text{hPa}} \{\overline{p}\}^{-(1-\kappa)}\left(-\left\{\partial_p\overline{\theta}\right\}\right)^{-1}\left(\{\overline{\theta}^2\} - \{\overline{\theta}\}^2\right)\, dp \quad (13)$$

where $\kappa = R/c_p$, R is the dry gas constant, c_p is the specific heat at constant pressure, g is the gravitational acceleration, $p_0 = 1000$ hPa is a reference pressure, $\{\cdot\}$ is an average over the NH extratropics (20° to 90°N), p_t is the tropopause pressure, and θ is potential temperature. We integrate from 850 hPa to p_t because it yields good agreement with the parcel moving algorithm of Stansifer et al. (2017, see Supplementary Fig. 2).

Following O'Gorman and Schneider (2008) we approximate the variance as $\left\{\overline{\theta}^2\right\} - \left\{\overline{\theta}\right\}^2 \approx \left\{\partial_y\overline{\theta}\right\}^2 L_Z/12$ where $\partial_y(\cdot) \equiv \partial(\cdot)/\partial\phi/a$ is the meridional gradient in spherical coordinates and L_Z is the meridional width of the baroclinic zone. Accordingly, MAPE is approximated as

$$MAPE \approx \frac{\kappa c_p}{24g}\frac{1}{p_0^{\kappa}}\int_{p_t}^{850\text{hPa}} \{\overline{p}\}^{-(1-\kappa)}\left(-\left\{\partial_p\overline{\theta}\right\}\right)^{-1}\left\{\partial_y\overline{\theta}\right\}^2 L_Z\, dp \quad (14)$$

and changes can be decomposed into baroclinicity and stability contributions, i.e.

$$\begin{aligned}\delta MAPE \approx\ & \frac{\kappa c_p}{24g}\frac{1}{p_0^{\kappa}}\int_{p_t}^{850\text{hPa}} \{\overline{p}\}^{-(1-\kappa)}\left(-\left\{\partial_p\overline{\theta}\right\}\right)^{-1}\delta\left\{\partial_y\overline{\theta}\right\}^2 L_Z\, dp \\ & + \frac{\kappa c_p}{24g}\frac{1}{p_0^{\kappa}}\int_{p_t}^{850\text{hPa}} \{\overline{p}\}^{-(1-\kappa)}\,\delta\left(-\left\{\partial_p\overline{\theta}\right\}\right)^{-1}\left\{\partial_y\overline{\theta}\right\}^2 L_Z\, dp. \quad (15)\\ \approx\ & \delta\text{Baro.} + \delta\text{Stab.} \quad (16)\end{aligned}$$

Since MAPE depends on the time- and zonal-mean temperature throughout the atmosphere, it cannot be predicted a priori for Snowball Earth.

2.3 Simulations

We focus on the Northern Hemisphere wintertime (December, January and February) storm track and simulate hard Snowball Earth and modern climates using two configurations of the ECHAM6 general circulation model (Stevens et al., 2013). The first configuration is a slab-ocean atmospheric general circulation model, hereafter referred to as AGCM. We simulate the modern climate with modern topography, obliquity, greenhouse gases (CO2 = 280 ppmv), a 50 m mixed layer depth and zero ocean energy transport. We simulate a hard Snowball Earth by imposing ice everywhere (ocean covered with sea ice and land covered with glaciers) in the modern simulation with an ice albedo of 0.6. The AGCM simulations are identical to those in Graham et al. (2019). Climate change in the AGCM is the difference of the Snowball Earth and modern simulations.

The second configuration is a slab-ocean aquaplanet general circulation model with modern obliquity, greenhouse gases, zero ocean energy transport, hereafter referred to as AQUA. The modern AQUA simulation has a 50 m mixed layer depth (Barpanda & Shaw, 2020; Donohoe et al., 2014). We simulate a hard Snowball Earth by varying the mixed layer depth from 50 m to 5 m with thermodynamic sea ice (a motionless single slab with no open water, Giorgetta et al., 2012) for a total of 14 simulations. (We use AQUA data from both wintertime hemispheres for a total of 28.) When the mixed layer depth is < 17.5 m we obtain a hard Snowball Earth (Supplementary Fig. 3) because the heat capacity becomes small enough to trigger a runaway ice-albedo feedback. The ice albedo is not prescribed in AQUA and can be greater than 0.6 because of the presence of snow on ice. Climate change in AQUA is the difference of Snowball Earth (15 m mixed layer depth) and modern (50 m mixed layer depth) simulations. The difference between the other mixed layer depth simulations and the modern simulation allow us to capture a range of climates between Snowball Earth and modern.

Since it is very common in the literature to perform slab-ocean aquaplanet simulations without thermodynamic sea ice (temperature can be below freezing without ice forming, Kang et al., 2008; Lee et al., 2008; Bordoni & Schneider, 2008; O'Gorman & Schneider, 2008), we perform a 15 m mixed layer depth simulation without sea ice and with a surface (ocean) albedo of 0.06 (Supplementary Fig. 4a) to quantify the importance of icy boundary conditions.

3 Results

3.1 Simulated Snowball Earth climate

Relative to the modern climate the Snowball Earth simulations have more ice (surface albedo$\geq$ 0.6, Fig. 1a), larger NH surface baroclinicity (equator minus pole surface temperature difference increases by 27 K in AGCM and 29 K in AQUA, Fig. 1b), weaker meridional surface MSE gradient (equator minus pole MSE difference decreases by 16 K in AGCM and 23 K in AQUA, Fig. 1c), weaker stationary eddy MSE flux (Fig. 1d) and weaker storm track intensity. The decreased meridional surface MSE gradient shows moisture dominates over temperature and a similar result holds for the near-surface (850 hPa) MSE. Storm track intensity is measured using the vertical integral of 1) transient eddy MSE flux (Fig. 1e) and 2) eddy kinetic energy (Fig. 1f).

The importance of icy boundary conditions for the Snowball Earth climate can be quantified by comparing the 15 m mixed layer depth AQUA simulations with and without sea ice. When sea ice is disabled surface baroclinicity and storm track intensity are both weaker than the modern simulation (Supplementary Fig. 4). This demonstrates a weak storm track-increased surface baroclinicity climate change can only be achieved with ice. Consistently, previous simulations without ice did not report a weak storm track-increased surface baroclinicity regime (O'Gorman & Schneider, 2008; Caballero & Langen, 2015).

3.2 Impact of hydrological cycle via surface boundary condition changes

According to the MSE framework, the weaker AGCM Snowball Earth storm track (δI, Fig. 2a) is associated with decreased turbulent heat flux (δI_{THF}, Fig. 2a), shortwave absorption (δI_{SWABS}, Fig. 2a) and greenhouse effect ($-\delta I_{GHE}$, Fig. 2a) contributions. The weakening of the storm track due to decreased latent heat flux (δI_{LHF}, Fig. 2a) dominates over the slight strengthening from sensible heat flux (difference between δI_{THF} and δI_{LHF}, Fig. 2a). The stationary circulation contribution ($-\delta I_{SC}$, Fig. 2a) also strengthens the storm track slightly consistent with stationary eddy-storm track compensation (Manabe & Terpstra, 1974; Barpanda & Shaw, 2017, see Figs. 1d and 1e). The contribution from atmospheric storage is small ($-\delta I_{\partial h/\partial t}$, Fig. 2a). Similar results are seen throughout the NH (Supplementary Fig. 5).

The weaker AQUA Snowball Earth storm track is also consistent with decreased turbulent heat flux (δI_{THF}, Fig. 2b) and shortwave absorption (δI_{SWABS}, Fig. 2b). Latent heat flux (δI_{LHF}, Fig. 2b) also dominates over sensible heat flux (difference between δI_{THF} and δI_{LHF}, Fig. 2b). The shortwave absorption contribution is larger in AQUA than in AGCM (compare δI_{SWABS}, Fig. 2a,b) consistent with the larger surface ice albedo in AQUA (Fig. 1a). The greenhouse effect contribution in AQUA is opposite of that in AGCM (compare $-\delta I_{GHE}$ Fig. 2a,b) due to land and clouds (Supplementary Fig. 6). Finally, the stationary circulation contribution in AQUA is also opposite of that in AGCM (compare $-\delta I_{SC}$, Fig. 2a,b) because it is dominated by the mean meridional circulation.

Is the weaker simulated Snowball Earth storm track relative to the modern climate consistent with the predicted weakening following hydrological cycle changes? Assuming the latent heat flux response decreases to 95% of its modern value ($\gamma \approx -0.95$) following the Clausius-Clapeyron relation [see (10)] over predicts the simulated weakening (compare δI_{THF} to $\delta I_{THF,p}$, Fig. 2a,b). The over prediction occurs because the latent heat flux decrease is less than 95% in the Southern Hemisphere ($\gamma > -0.95$) and the change in sensible heat flux is non-negligible (Supplementary Fig. 1a,b). Assuming the shortwave optical depth decreases following the Clausius-Clapeyron ($\tau_S \approx 0.05\tau_M$) and there is a surface ice albedo everywhere [see (12)] over predicts the simulated weakening in AGCM (compare δI_{SWABS} to $\delta I_{SWABS,p}$, Fig. 2a) but accurately predicts it in AQUA (compare δI_{SWABS} to $\delta I_{SWABS,p}$, Fig. 2b). The AGCM over prediction is once again associated with the response in the Southern Hemisphere (Supplementary Fig. 1c,d) where the decrease of summertime shortwave optical depth is greater than 5%, i.e. $\tau_S > 0.05\tau_M$, and there are important meridional changes in planetary albedo. Finally, δI_{GHE}, δI_{SC} and $\delta I_{\partial h/\partial t}$ are small as expected.

Across the range of climates between modern and Snowball Earth in AQUA, the storm track intensity change follows the turbulent heat flux contribution (δI_{THF}, Fig. 2c). The shortwave absorption contribution exhibits a nonlinear relationship with intensity changes (δI_{SWABS}, Fig. 2c) and the greenhouse effect contribution exhibits the opposite sign ($-\delta I_{GHE}$, Fig. 2c). Thus, turbulent heat fluxes not only control the weakening of the storm track between the Snowball Earth and modern climates but also across a range of climates in between.

Overall, the MSE framework shows the weaker Snowball Earth storm track relative to the modern climate is consistent with the impact of the hydrological cycle via changes in surface boundary conditions. In particular, the cold, dry and icy conditions decrease the latent heat flux and shortwave absorption in the tropics relative to the poles, which leads to a weaker equator-to-pole net energy input gradient and thereby a weaker storm track. Furthermore the weakening can be predicted following the Clausius-Clapeyron relation and assuming a surface ice albedo because the greenhouse effect, stationary circulation, and atmospheric storage contributions are small. The weaker equator-to-pole latent heat flux (evaporation) gradient is consistent with the decreased meridional MSE gradient at the surface (Fig. 1c) and aloft (Fig. 2d,e).

3.3 Impact of hydrological cycle via changes in thermal structure

Next we examine how the transition to the cold and dry Snowball Earth climate impacts storm track intensity, as measure by eddy kinetic energy, via changes in the thermal structure of the atmosphere that affect MAPE. The weaker storm track in the AGCM Snowball Earth simulation relative to modern is consistent with weaker MAPE (δMAPE, square, Fig. 3a), which is dominated by the change in baroclinicity (δBaro., square, Fig. 3a) rather than stability (δStab., square, Fig. 3a). When examining the range of climates between modern and Snowball Earth in AQUA, the storm track intensity change relative to modern also follows MAPE ($\delta MAPE$, Fig. 3a), which is mostly dominated by changes in baroclinicity (δBaro., Fig. 3a) rather than stability (δStrat., Fig. 3a).

Since surface baroclinicity does not account for the weaker Snowball Earth storm track relative to the modern climate (Fig. 1a), the MAPE results suggest upper-tropospheric baroclinicity is important. Indeed the temperature difference between the Snowball Earth and modern simulations involve weaker upper-tropospheric baroclinicity connected to greater tropical cooling aloft (Fig. 3b,c).

3.4 Connecting storm track intensity to other variables

The surface baroclinicity-intensity connection is appealing because it connects storm track intensity (a turbulent quantity) to the meridional surface temperature gradient (a mean quantity), which can be inferred from paleo proxy data. However, storm track intensity is not significantly correlated with surface baroclinicity across the AQUA and AGCM simulations ($R = 0.01$, Fig. 4a). A similar result holds for near-surface (850 hPa) temperature ($R = 0.20$, Fig. 4b). Note this only occurs in the presence of ice. O'Gorman and Schneider (2008) and Caballero and Langen (2015) documented a linear relationship between surface baroclinicity and storm track intensity in the absence of ice.

The impact of the hydrological cycle via surface boundary condition and thermal structure changes suggests other variables may be more important than surface temperature. For example, the MSE framework shows the weaker simulated Snowball Earth storm track is consistent with decreased latent heat flux, which affects near-surface MSE via moisture changes. Consistently, storm track intensity exhibits a significant correlation with equator minus pole surface MSE ($R = 0.94$, Fig. 4c). Assuming surface temperature is given, e.g. inferred from paleo proxy data, the equator minus pole surface MSE can be estimated using the Clausius-Clapeyron relation and is significantly correlated with storm track intensity ($R = 0.94$, Supplementary Fig. 7a).

The MAPE framework shows the weaker Snowball Earth storm track is consistent with decreased upper-tropospheric baroclinicity. Consistently, upper-tropospheric (500 hPa) baroclinicity exhibits a significant correlation with storm track intensity ($R = 0.98$, Fig. 4d) and MAPE (Supplementary Fig. 7b). Upper-tropospheric baroclinicity follows the impact of reduced latent heat release aloft in the tropics estimated via the moist adiabat (Supplementary Fig. 7c) and is significantly correlated with equator minus pole surface MSE ($R = 0.98$). In contrast upper-tropospheric and surface baroclinicity are not significantly correlated ($R = 0.10$). Thus, hydrological cycle changes, which impact the meridional surface MSE (moisture) gradient and consequently the thermal structure aloft via convective adjustment, are more important than surface temperature changes for storm track intensity across the range of climates between modern and Snowball Earth.

4 Discussion

Snowball Earth is an exotic climate with a radically different hydrological cycle than the modern Earth. Here we examined whether zonally-symmetric hydrological cycle changes that impact surface boundary conditions and thermal structure can account for the weaker

Snowball Earth storm track despite increased surface baroclinicity. The MSE framework shows that surface boundary condition changes weaken the Snowball Earth storm track via decreased turbulent heat flux (decreased evaporation) and shortwave absorption (decreased shortwave optical depth and increased surface albedo), which decrease the equator-to-pole gradient of net energy input and the meridional surface MSE gradient. A weaker storm track can be predicted assuming the hydrological cycle changes follow the Clausius-Clapeyron relation and there is a surface ice albedo everywhere. The weaker storm track is also consistent with decreased latent heat release aloft in the tropics, which decreases upper-tropospheric baroclinicity and MAPE, and is significantly correlated with the meridional surface MSE gradient. Thus, hydrological cycle changes can explain the weak Snowball Earth storm track despite increased surface baroclinicity because the intensity follows the meridional surface MSE (and upper-tropospheric temperature) gradient and, importantly, not the surface temperature gradient.

Our results are consistent with Lapeyre and Held (2004) who showed lower-layer MSE is most appropriate for diffusive models of energy transport in idealized moist two-layer simulations. Future work must focus on understanding the importance of the moisture versus eddy kinetic energy decrease for the energy transport, including its connection to diffusivity changes. The results imply EBM studies of Snowball Earth should be based on the atmospheric MSE budget, i.e. an equation for surface MSE, and not on the TOA energy budget, i.e. an equation for surface temperature. Several studies have shown MSE based fixed-diffusivity EBMs capture the climate response to increased CO2 concentration (Hwang & Frierson, 2010; Roe et al., 2015; Siler et al., 2018; Armour et al., 2019). Our results are also consistent with previous work that highlighted the importance of upper-tropospheric baroclinicity changes for the storm track intensity response to increased CO2 (O'Gorman, 2010; Harvey et al., 2015).

Here we showed zonally-symmetric changes in the hydrological cycle can explain the weak Snowball Earth storm track despite increased surface baroclinicity. Previous work explained the weak LGM North Atlantic storm track using zonally-asymmetric dry dynamical mechanisms connected to orographic forcing. Assessing whether hydrological cycle changes can also account for the weak LGM North Atlantic storm track requires extending the MSE framework for storm track intensity to the North Atlantic basin as well as quantifying the importance of orography versus latent heat flux and surface albedo changes (cf. Roberts & Valdes, 2017), which is work in progress. If the Snowball Earth results hold for other paleoclimates then estimates of paleo surface MSE gradients (combining paleo proxy temperatures and the Clausius-Clapeyron relation) could potentially be used to estimate paleo storm track intensity.

Acknowledgments

TAS acknowledges support from NSF (AGS-1742944) and RJG acknowledges scholarship funding from the Clarendon Fund and Jesus College, Oxford. The authors thank two anonymous reviewers for their helpful comments. TAS thanks Paul O'Gorman for providing code to calculate MAPE using the parcel-moving algorithm and Osamu Miyawaki for providing code to calculate the moist adiabat. The simulations in this paper were completed with resources provided by the University of Chicago Research Computing Center. Data and code necessary to reproduce the figures in this paper are available via The University of Chicago's institutional repository Knowledge@UChicago (10.6082/uchicago.2201).

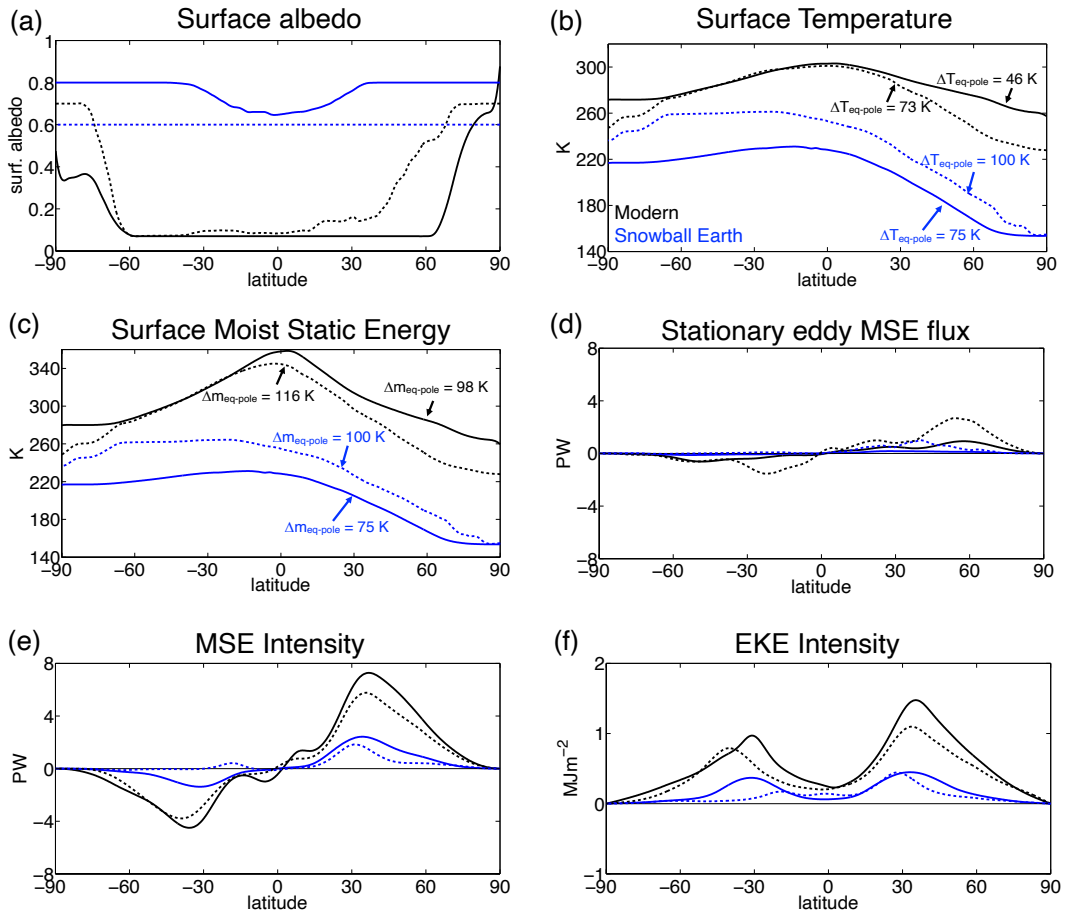

Figure 1. Northern Hemisphere wintertime (a) surface albedo, (b) surface temperature, (c) surface MSE (divided by specific heat at constant pressure), (d) stationary eddy MSE flux and storm track intensity defined by vertically-integrated (e) transient eddy MSE flux and (f) eddy kinetic energy for AGCM (dashed) and AQUA (solid) modern (black) and Snowball Earth (blue) simulations.

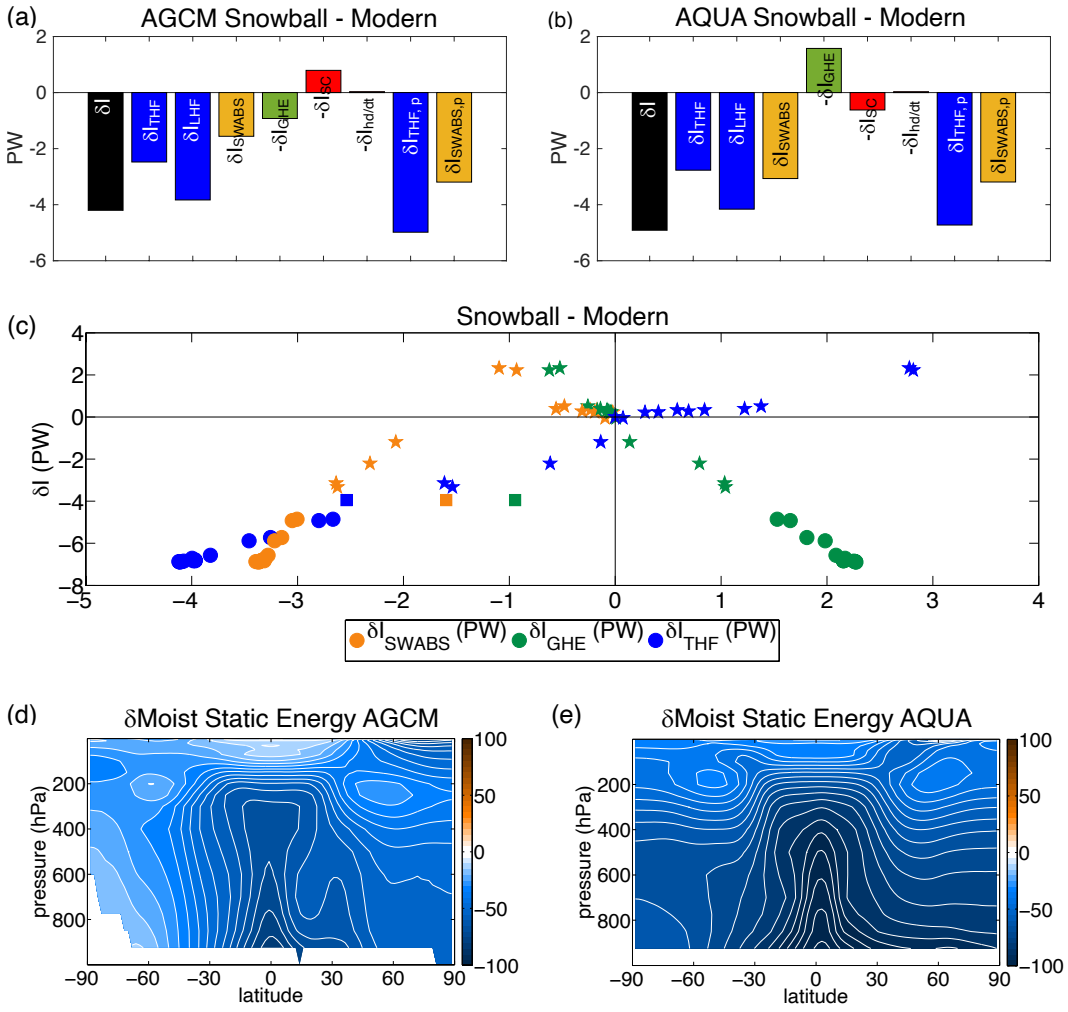

Figure 2. (a,b) Weakening of Northern Hemisphere wintertime storm track intensity between Snowball Earth and modern (δI in PW) at the storm track position decomposed into turbulent heat flux (δI_{THF}), latent heat flux (δI_{LHF}), shortwave absorption (δI_{SWABS}), greenhouse effect ($-\delta I_{GHE}$), stationary circulation ($-\delta I_{SC}$) and atmospheric storage ($-\delta I_{\partial h/\partial t}$) contributions following the MSE framework. Predicted values have a 'p' subscript. The response of storm track intensity relative to modern (δI in PW) decomposed as in (a,b). AGCM simulations shown by squares and AQUA simulations shown by stars and circles with circles denoting Snowball simulations. (d,e) Difference of time- and zonal-mean MSE (divided by specific heat at constant pressure) between Snowball Earth and modern simulations. Contour interval is 5 K

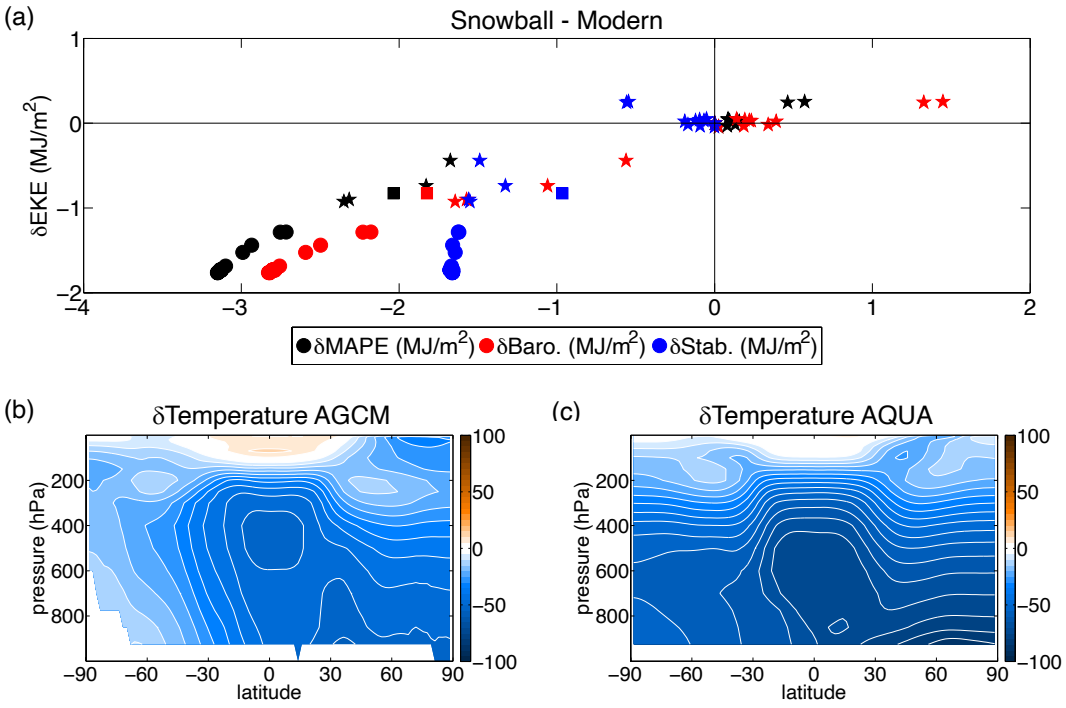

Figure 3. (a) Weakening of Northern Hemisphere wintertime eddy kinetic energy storm track intensity integrated over the extratropics (δEKE in MJm^{-2}) as a function of MAPE changes (δMAPE) and their decomposition into baroclinicity (δBaro.) and stability (δStab.) contributions. AGCM simulations shown by squares and AQUA simulations shown by stars and circles with circles denoting Snowball simulations. (b,c) Difference of time- and zonal-mean temperature between Snowball Earth and modern simulations. Contour interval is 5 K.

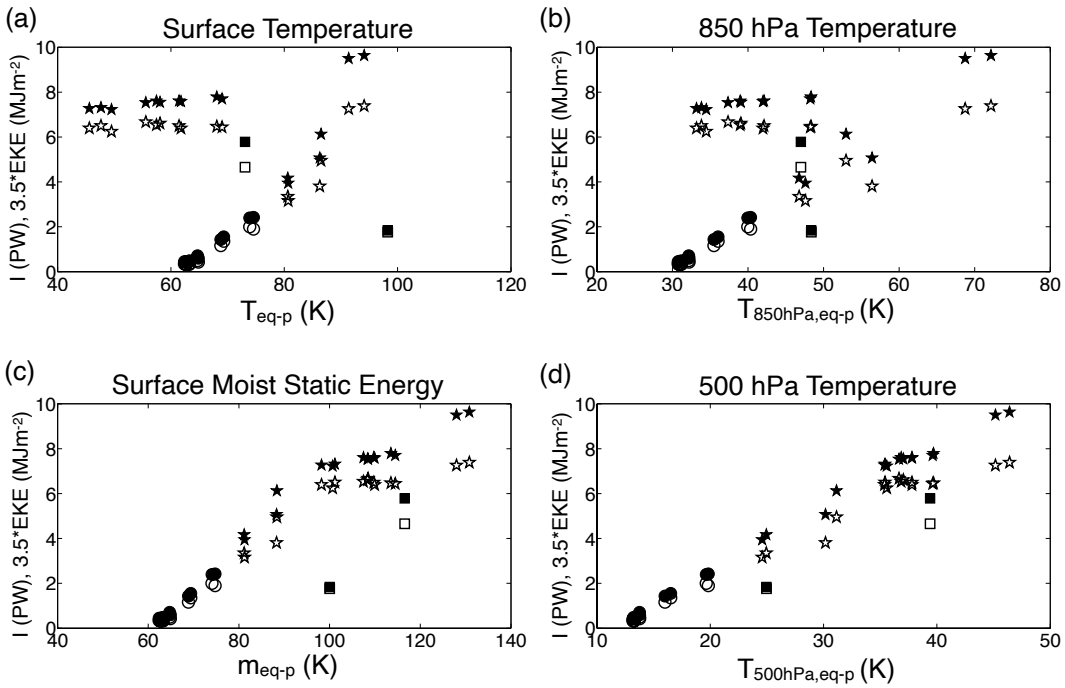

Figure 4. Storm track intensity versus equator minus pole (a) surface (2 m) temperature (b) 850 hPa temperature, (c) surface (2 m) MSE and (d) 500 hPa temperature. MSE and EKE (multiplied by 3.5) intensity indicated by closed and open symbols, respectively. AGCM simulations shown by squares and AQUA simulations shown by stars and circles with circles denoting Snowball simulations.

References

Armour, K. C., Siler, N., Donohoe, A., & Roe, G. H. (2019). Meridional atmospheric heat transport constrained by energetics and mediated by large-scale diffusion. *J. Climate*, *32*, 3655–3680.

Barpanda, P., & Shaw, T. A. (2017). Using the moist static energy budget to understand storm-track shifts across a range of time scales. *J. Atmos. Sci.*, *74*(8), 2427–2446.

Barpanda, P., & Shaw, T. A. (2020). Surface fluxes modulate the seasonality of zonally-mean storm tracks. *J. Atmos. Sci.*, *77*, 753–779.

Boos, W. R. (2012). Thermodynamic scaling of the hydrological cycle of the Last Glacial Maximum. *J. Climate*, *25*, 992-1006.

Bordoni, S., & Schneider, T. (2008). Monsoons as eddy-mediated regime transitions of the tropical overturning circulation. *Nature Geosc.*, *1*(8), 515.

Caballero, R., & Langen, P. L. (2015). The dynamic range of poleward energy transport in an atmospheric general circulation model. *Geophys. Res. Lett.*. doi: 10.1029/2004GL021581

Chang, E., Lee, S., & Swanson, K. K. (2002). Storm track dynamics. *J. Climate*, *15*, 2163–2183.

Donohoe, A., Armour, K. C., Roe, G. H., Battisti, D. S., & Hahn, L. (2020). The partitioning of meridional heat transport from the last glacial maximum to CO2 quadrupling in coupled climate models. *J. Climate*, *33*, 4793-4808.

Donohoe, A., & Battisti, D. S. (2009). Causes of reduced North Atlantic storm activity in a CAM3 simulation of the last glacial maximum. *J. Climate*, *22*, 4793-4808.

Donohoe, A., & Battisti, D. S. (2012). What determines meridional heat transport in climate models? *J. Climate*, *25*, 3832-3850.

Donohoe, A., Frierson, D. M. W., & Battisti, D. S. (2014). The effect of ocean mixed layer depth on climate in slab ocean aquaplanet experiments. *Clim. Dynamics*, *43*, 1041–1055.

Gertler, C. G., & O'Gorman, P. A. (2019). Changing available energy for extratropical cyclones and associated convection in Northern Hemisphere summer. *Proc. Nat. Acad. Sci.*. doi: 10.1073/pnas.1812312116

Giorgetta, M. A., Roeckner, E., Mauritsen, T., Stevens, B., Bader, J., Crueger, T., ... Krismer, T. (2012). The atmospheric general circulation model echam6: Model description. *Max Planck Institute for Meteorology, Hamburg, Germany*. Retrieved from `https://icdc.cen.uni-hamburg.de/fileadmin/user_upload/icdc_Dokumente/ECHAM/echam6_scidoc.pdf`

Graham, R. J., Shaw, T. A., & Abbot, D. S. (2019). The snowball stratosphere. *J. Geophys. Res.*. doi: 10.1029/2019JD031361

Hall, N. M. J., Dong, B., & Valdes, P. J. (1996). Atmospheric equilibrium, instability and energy transport at the Last Glacial Maximum. *Climate Dyn.*, *12*, 197–511.

Harvey, B. J., Shaffrey, L. C., & Woollings, T. J. (2015). Deconstructing the climate change response of the Northern Hemisphere wintertime storm tracks. *Clim. Dyn.*, *45*, 2847-2860.

Held, I. M. (2018). 100 years of progress in understanding the general circulation of the atmosphere. *Meteorological Monographs*, *59*. doi: 10.1175/AMSMONOGRAPHS-D-18-0017.1

Held, I. M., & Soden, B. J. (2006). Robust responses of the hydrological cycle to global warming. *J. Climate*, *19*, 5686-5699.

Hoffman, P. F., Abbot, D. S., Ashkenazy, Y., Benn, D. I., Brocks, J. J., Cohen, P. A., ... Warren, S. G. (2017). Snowball Earth climate dynamics and cryogenian geology-geobiology. *Science Advances*. doi: 10.1126/sciadv.1600983

Hwang, Y.-T., & Frierson, D. M. W. (2010). Increasing atmospheric poleward energy transport with global warming. *Geophys. Res. Lett.*, *37*. doi: 10.2951029/

2010GL045440

Kang, S. M., Held, I. M., Frierson, D. M. W., & Zhao, M. (2008). The response of the ITCZ to extratropical thermal forcing: Idealized slab-ocean experiments with a GCM. *J. Climate*, *21*, 3521–3532.

Lapeyre, G., & Held, I. M. (2004). The role of moisture in the dynamics and energetics of turbulent baroclinic eddies. *J. Atmos. Sci.*, *61*, 1693–1710.

Lee, M.-I., Suarez, M. J., Kang, I.-S., Held, I. M., & Kim, S. (2008). A moist benchmark calculation for atmospheric general circulation models. *J. Climate*, *21*, 4934–4954.

Li, C., & Battisti, D. S. (2008). Reduced Atlantic storminess during Last Glacial Maximum: Evidence from a coupled climate model. *J. Climate*, *21*, 3561–3579.

Lofverstrom, M., Caballero, R., Nilsson, J., & Messori, G. (2016). Stationary wave reflection as a mechanism for zonalising the Atlantic winter jet at the LGM. *J. Atmos. Sci.*, *73*, 3329-3342.

Manabe, S., & Terpstra, T. B. (1974). The effects of mountains on the general circulation of the atmosphere as identified by numerical experiments. *J. Atmos. Sci.*, *31*, 3–42.

Mbengue, C., & Schneider, T. (2018). Linking Hadley circulation and storm tracks in a conceptual model of the atmospheric energy balance. *J. Atmos. Sci.*, *75*(3), 841–856.

North, J. R. (1975). Theory of energy-balance climate models. *J. Atmos. Sci.*, *32*, 1189-1204.

O'Gorman, P. A. (2010). Understanding the varied response of the extratropical storm tracks to climate change. *Proc. Nat. Acad. Sci.*, *107*, 19176–19180.

O'Gorman, P. A., & Schneider, T. (2008). Energy of midlatitude transient eddies in idealized simulations of changed climates. *J. Climate*, *21*, 5797–5806.

Pierrehumbert, R. T. (2002). The hydrologic cycle in deep-time climate problems. *Nature*, *419*, 191–198.

Pierrehumbert, R. T. (2005). Climate dynamics of a hard Snowball Earth. *J. Geophys. Res.*, *110*. doi: 10.1029/2004JD005162

Riviere, G., Berthou, S., Lapeyre, F., & Kageyama, M. (2018). On the reduced North Atlantic storminess during the last glacial period: The role of topography in shaping synoptic eddies. *J. Climate*, *31*, 1637-1638.

Roberts, W. H. G., & Valdes, P. J. (2017). Green mountains and white plains: The effect of Northern Hemisphere ice sheets on the global energy budget. *J. Climate*, *30*, 3887-3905.

Roe, G. H., Feldl, N., Armour, K. C., Hwang, Y.-T., & Frierson, D. M. W. (2015). Regional climate predictability from regional feedbacks. *Nature Geosc.*. doi: 10.1038/NGEO2346

Schneider, T., O'Gorman, P. A., & Levine, X. J. (2010). Water vapor and the dynamics of climate changes. *Reviews of Geophysics*, *48*. doi: 10.1029/2009RG000302

Shaw, T. A., Baldwin, M., Barnes, E. A., Caballero, R., Garfinkel, C. I., Hwang, Y.-T., ... Voigt, A. (2016). Storm track processes and the opposing influences of climate change. *Nature Geosc.*, *9*, 656–664.

Shaw, T. A., Barpanda, P., & Donohoe, A. (2018). A moist static energy framework for zonal-mean storm-track intensity. *J. Atmos. Sci.*, *75*(6), 1979–1994.

Siler, N., Roe, G. H., & Armour, K. C. (2018). Insights into the zonal-mean response of the hydrologic cycle to global warming from a diffusive energy balance model. *J. Climate*, *31*, 7481–7493.

Stansifer, E. M., O'Gorman, P. A., & Holt, J. L. (2017). Accurate computation of moist available potential energy with the Munkres algorithm. *Q. J. R. Meteorol. Soc.*, *143*, 288-292.

Stevens, B., Giorgetta, M., Esch, M., Mauritian, T., Crueger, T., Rast, S., ...

Roeckner, E. (2013). Atmospheric component of the MPI-M Earth System Model: ECHAM6. *J. Adv. Model. Earth Syst.*, *5*, 146–172.

Figure 1.

(a) Surface albedo

surf. albedo

latitude

(b) Surface Temperature

K

latitude

$\Delta T_{eq\text{-}pole}$ = 46 K

$\Delta T_{eq\text{-}pole}$ = 73 K

$\Delta T_{eq\text{-}pole}$ = 100 K

$\Delta T_{eq\text{-}pole}$ = 75 K

Modern

Snowball Earth

(c) Surface Moist Static Energy

K

latitude

$\Delta m_{eq\text{-}pole}$ = 116 K

$\Delta m_{eq\text{-}pole}$ = 98 K

$\Delta m_{eq\text{-}pole}$ = 100 K

$\Delta m_{eq\text{-}pole}$ = 75 K

(d) Stationary eddy MSE flux

PW

latitude

(e) MSE Intensity

PW

latitude

(f) EKE Intensity

MJm^{-2}

latitude

Figure 2.

(a)

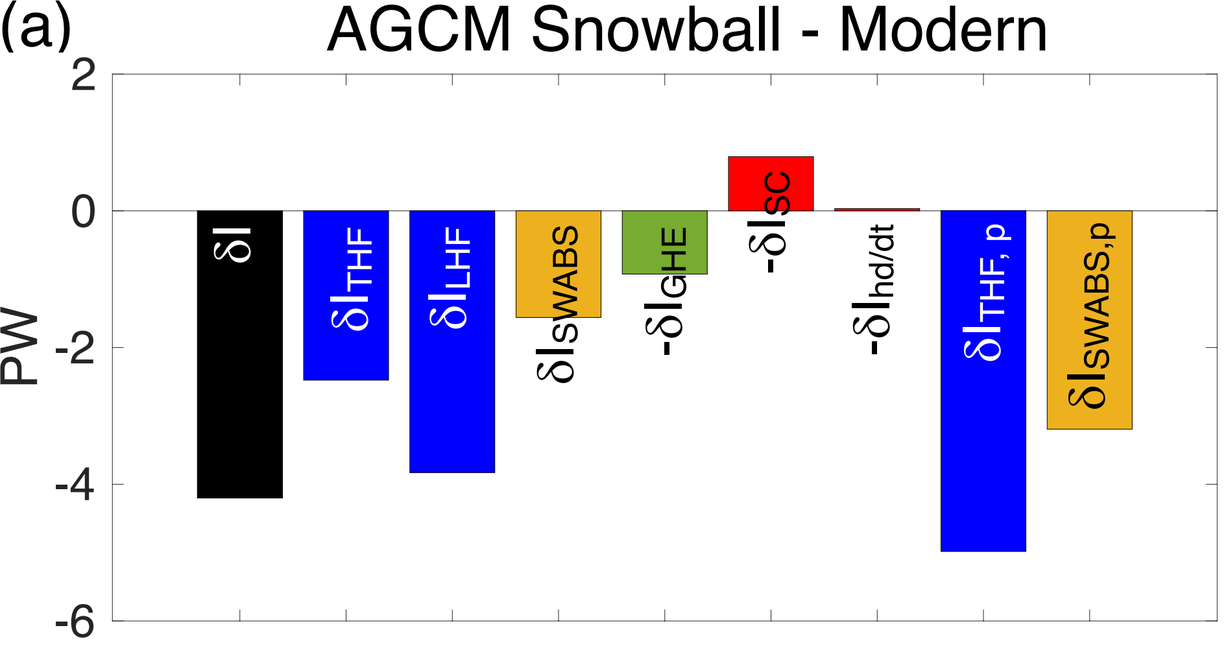
AGCM Snowball - Modern
PW
2
0
-2
-4
-6
δI
δI_THF
δI_LHF
δI_SWABS
-δI_GHE
-δI_SC
-δI_hd/dt
δI_THF, p
δI_SWABS,p

(b)

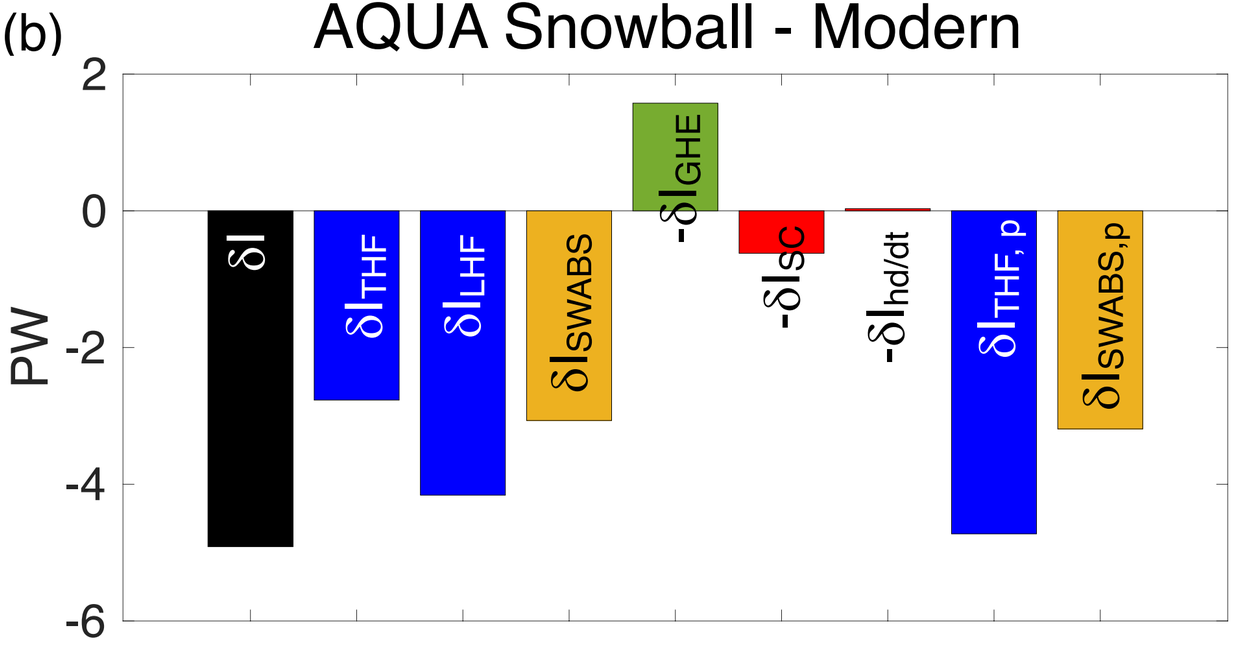
AQUA Snowball - Modern
PW
2
0
-2
-4
-6
δI
δI_THF
δI_LHF
δI_SWABS
-δI_GHE
-δI_SC
-δI_hd/dt
δI_THF, p
δI_SWABS,p

(c)

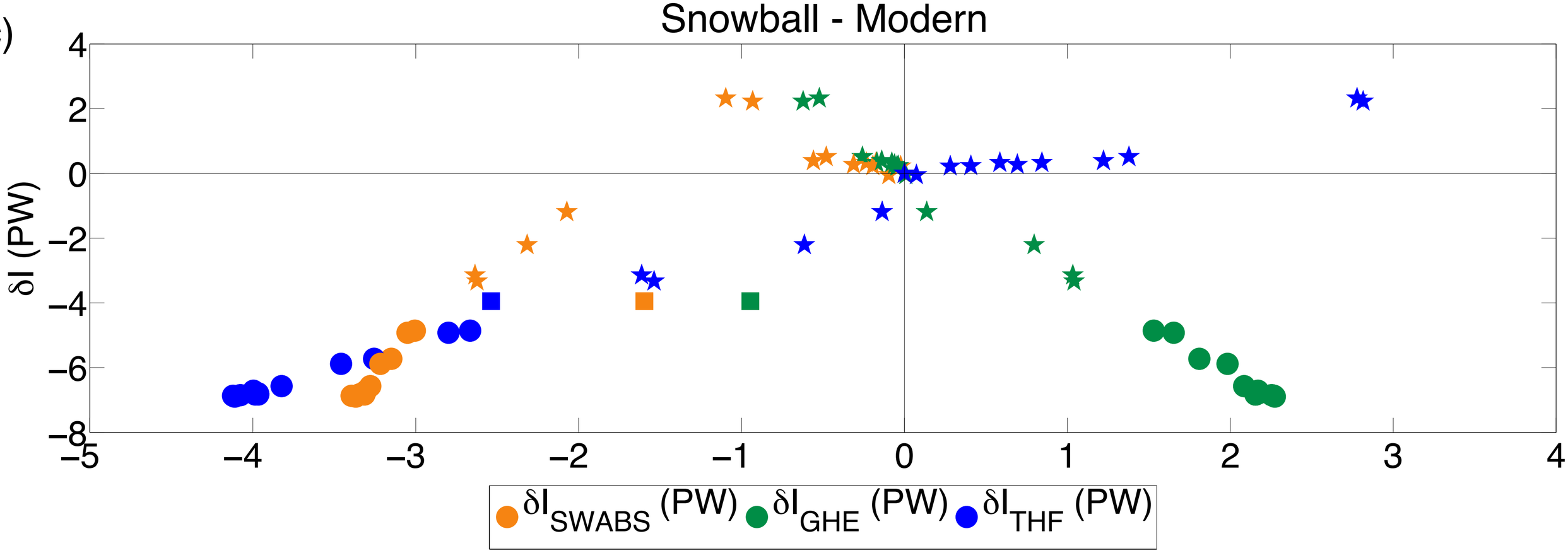
Snowball - Modern
δI (PW)
4
2
0
−2
−4
−6
−8
−5
−4
−3
−2
−1
0
1
2
3
4
δI_SWABS (PW)
δI_GHE (PW)
δI_THF (PW)

(d)

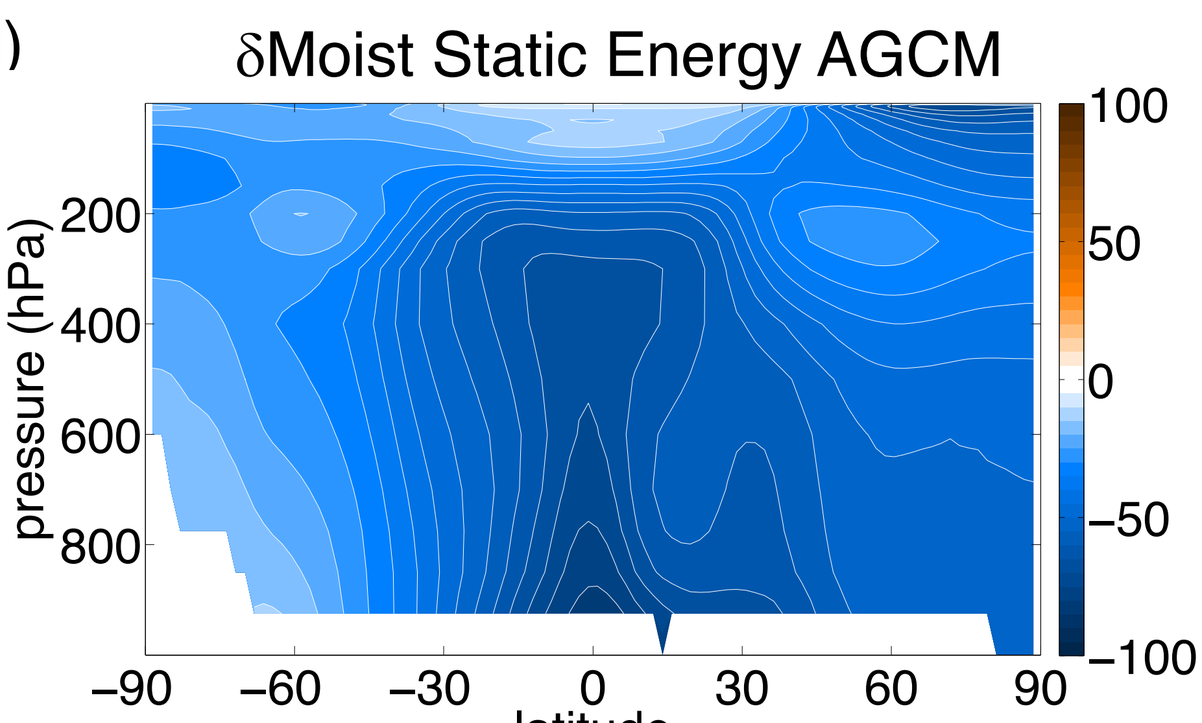
δMoist Static Energy AGCM
pressure (hPa)
200
400
600
800
−90
−60
−30
0
30
60
90
latitude
100
50
0
−50
−100

(e)

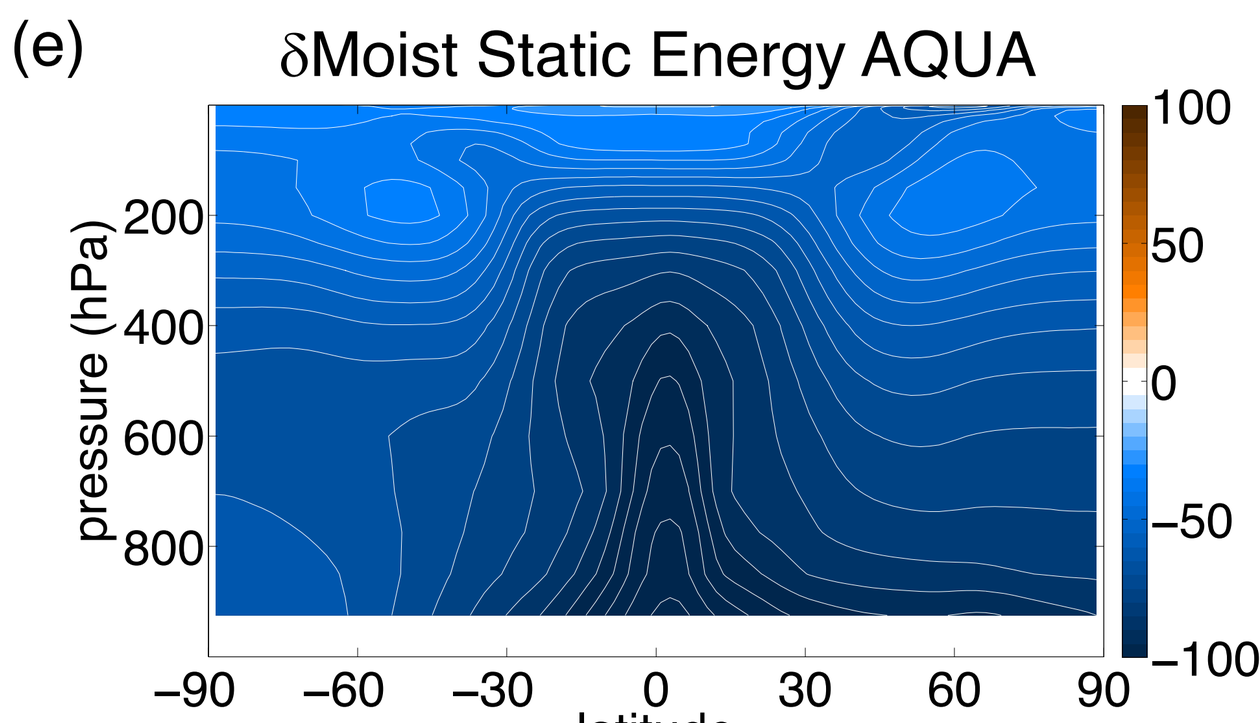
δMoist Static Energy AQUA
pressure (hPa)
200
400
600
800
−90
−60
−30
0
30
60
90
latitude
100
50
0
−50
−100

Figure 3.

(a)

Snowball - Modern

δEKE (MJ/m^2)

δMAPE (MJ/m^2) δBaro. (MJ/m^2) δStab. (MJ/m^2)

(b)

δTemperature AGCM

pressure (hPa)

latitude

(c)

δTemperature AQUA

pressure (hPa)

latitude

Figure 4.

(a)

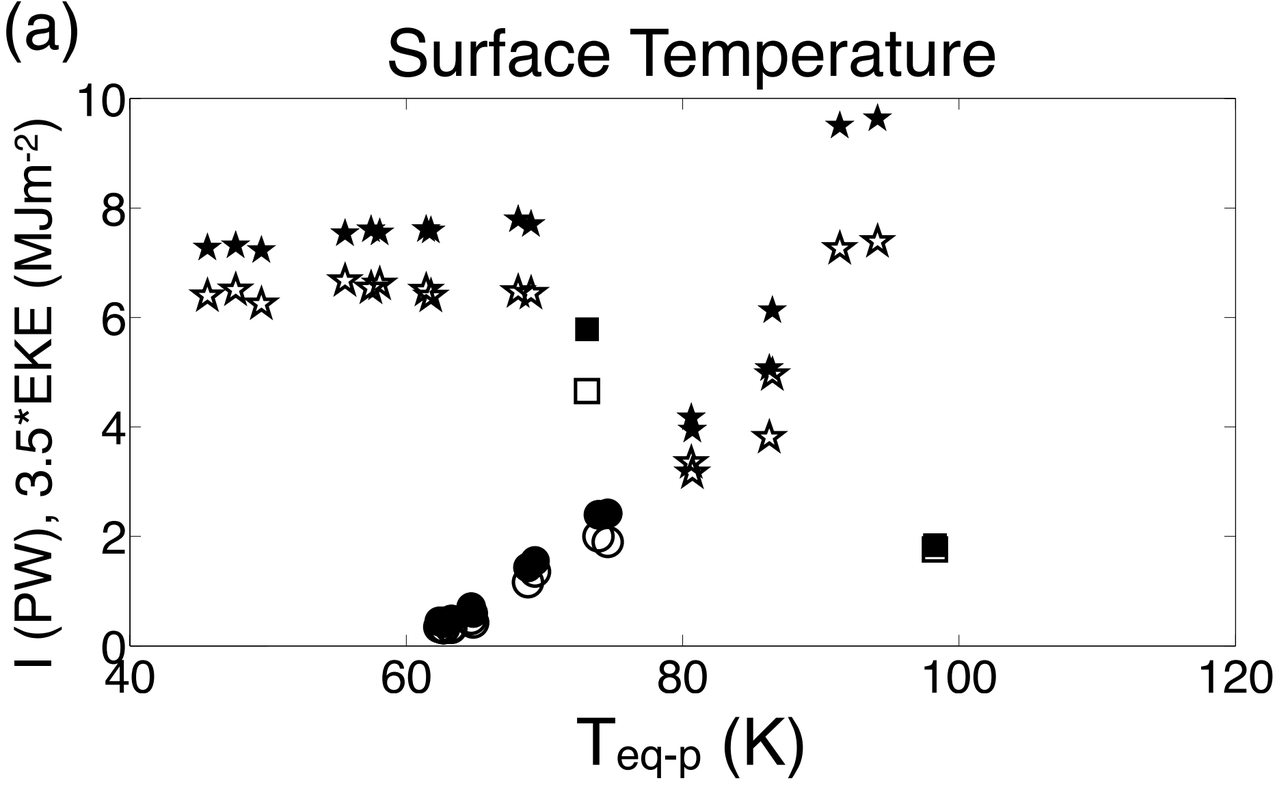
Surface Temperature
I (PW), 3.5*EKE (MJm-2)
Teq-p (K)
0
2
4
6
8
10
40
60
80
100
120

(b)

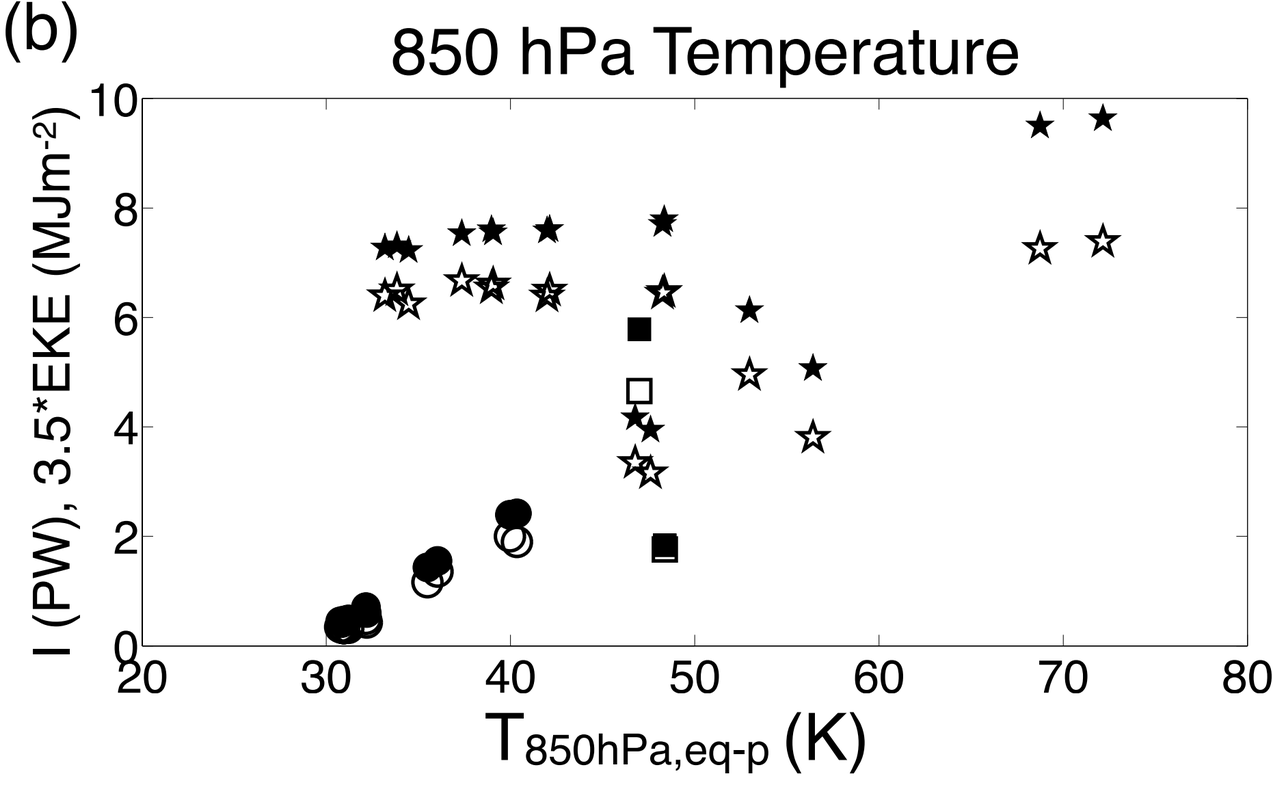
850 hPa Temperature
I (PW), 3.5*EKE (MJm-2)
T850hPa,eq-p (K)
0
2
4
6
8
10
20
30
40
50
60
70
80

(c)

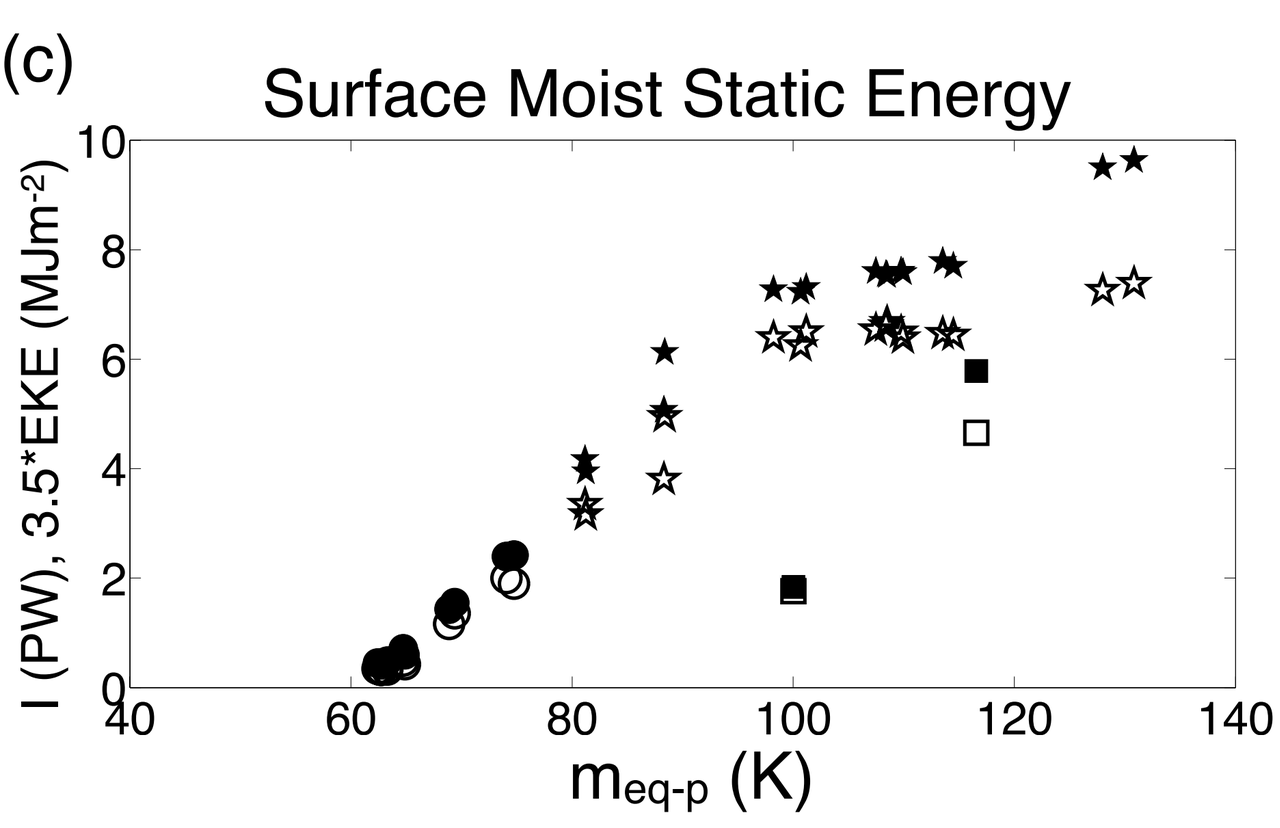
Surface Moist Static Energy
I (PW), 3.5*EKE (MJm-2)
meq-p (K)
0
2
4
6
8
10
40
60
80
100
120
140

(d)

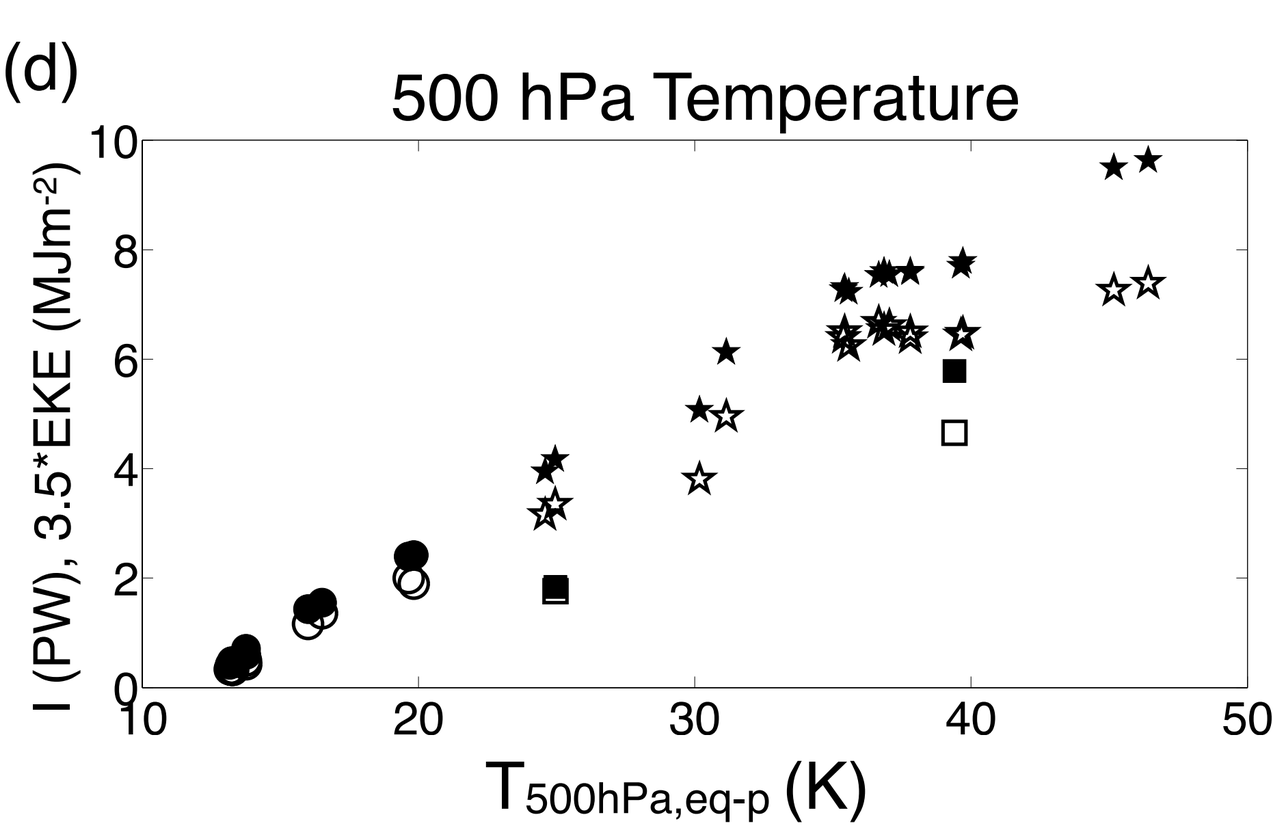
500 hPa Temperature
I (PW), 3.5*EKE (MJm-2)
T500hPa,eq-p (K)
0
2
4
6
8
10
10
20
30
40
50